SPE 94097

Interpretation of Temperature and Pressure Profiles Measured in Multilateral Wells Equipped with Intelligent Completions

K. Yoshioka, D. Zhu, and A.D. Hill, Texas A&M U., and L.W. Lake, U. of Texas at Austin

This paper was prepared for presentation at the SPE Europec/EAGE Annual Conference held in Madrid, Spain, 13-16 June 2005.

Abstract

This paper presents methods to interpret measurements in complex wells (horizontal, multilateral and multi-branching wells) to determine the inflow profiles of oil, gas and water. These methods are needed to take full advantage of intelligent well, a technology that is rapidly evolving to continuously and permanently monitor downhole temperature, pressure, and perhaps volumetric flow. To realize the value of intelligent wells, the efficient and accurate interpretation of the raw data being acquired is needed.

The interpretation of flow profiles of horizontal or multilateral wells from temperature and pressure profiles requires consideration of subtle effects that are often neglected. In this paper, we illustrate how some of these effects can be predicted, and how they can be used to evaluate complex well performance. In particular, we will highlight the following characteristics of flow in horizontal wells, each of which can provide information about the inflow profile of the well.

Firstly we discuss about Joule-Thomson effects (the heating of oil and the cooling of gas) on the temperature profiles, seeing if they are noticeable changes or not. The discrete production cases are then considered to infer how the pressure or temperature profiles retain marks where the production starts and ends. Also, we examine well trajectories effects. Small inclinations ($+2^o$ and -2^o) in nominally horizontal laterals affect both pressure and temperature profiles. The differences in potential energy in up-inclined and down-inclined segments may prove to be diagnostic of relative flow rates of the phases. As a last example, water entry effects on the each profiles are shown. When the production becomes oil and water two-phase flow, the fluid properties change and affect the both profiles. In certain cases, the location of the water entry may be noticeable.

Introduction

Distributed temperature sensor (DTS) technology is increasingly applied as a downhole measurement method for complex wells. DTS supplies real-time temperature profile measurements that can be used to identify fluid entries and perhaps quantify the flow rate profile.

In vertical or near vertical wells, the wellbore pressure is usually dominated by hydrostatic difference, and the wellbore temperature by the geothermal temperature; both of which change with depth. However, for horizontal or near horizontal wells, the hydrostatic difference is very small and formation temperature is almost constant. Thus, we must consider second-order effects, which are usually negligible in vertical wells to predict temperature and pressure profiles.

One of the earliest works on temperature prediction was done by Ramey[1]. His temperature prediction model works for either a single phase incompressible liquid or a single phase ideal gas in vertical injection and production wells. His method has been extended and revised by other authors[2,3]. However, there has been little work on the thermal modeling of horizontal producing wellbores. As we will show later, one reason for this is that to a good approximation a horizontal wellbore can be considered isothermal because it is exposed to about same geothermal temperature and the changes resulting from flow are very small.

Several studies[4-6] have addressed the pressure profiles in horizontal wells. Even when there is no gravitational pressure drop, regarding wellbore pressure as constant results in errors in estimated production profiles. Flow in a horizontal wellbores consists of two streams that are in the axial direction (along the wellbore) and the radial direction (from the reservoir). Simultaneously, the radial stream is a function of wellbore pressure. A higher pressure drop in the wellbore causes more inflow from the formation; and the larger the inflow, the larger the pressure drop along the wellbore. Therefore the modeling of the pressure behavior in horizontal wells requires careful treatment. Temperature modeling requires even more care because of their subtle changes.

Our objective of this study is to develop a prediction model that can generate flow rate, pressure and temperature profiles along the wellbore based on the reservoir and the surface conditions. The model developed can be used in sensitivity studies to identify the flow profile parameters that affect temperature and pressure profiles in a recognizable

fashion. Results from the model would indicate how best to infer inflow profiles from DTS data.

Prediction Model

To solve for the temperature profile along the wellbore, the flow rate and pressure profiles are needed. Flow rate should be obtained by the reservoir and wellbore conditions and formation temperature is given as a boundary condition.

Working Equations. Consider a volume element of a wellbore that produces fluids from the formation as illustrated in Fig. 1. Mass, momentum and total energy balances are applied over a volume element on a macroscopic scale.

Mass Balance Equation. Conservation of mass can be derived by observing the incoming mass flux, outgoing mass flux and accumulated mass in the volume element, then,

$$\pi R^2 \frac{\partial(\rho_i y_i)}{\partial t} = -\pi R^2 \frac{\partial(\rho_i v_i y_i)}{\partial x} + 2\pi R\gamma \rho_{i,I} v_{i,I} y_{i,I} \qquad (1)$$

where the subscript i stands for the phases and subscript I represents an inflowing fluid property. Then v_i is a velocity along the wellbore and $v_{i,I}$ is an inflow flux as shown in Fig. 1. R is a pipe radius, y_i is a holdup of the phase. $2\pi R\gamma$ gives the opened pipe area and γ is the pipe opening ratio, defined here as

$$\gamma = \frac{\text{Opened pipe surface area}}{\text{Pipe surface area}} \qquad (2)$$

Momentum Balance Equation. Conservation of momentum in the axial direction can be obtained by equating net force on the volume element to momentum change as

$$\frac{\partial(\rho_m v_m)}{\partial t} = -\frac{2\tau_w}{R} - \frac{\partial\left(\rho_m {v_m}^2 + p\right)}{\partial x} - \rho_m g \sin\theta \qquad (3)$$

where τ_w is the wall shear stress. The pressures for each phase are assumed to be equal. ρ_m and v_m are the mixture (fluid) density and velocity respectively defined as

$$\rho_m = \sum_i \rho_i y_i \qquad (4)$$

and

$$v_m = \frac{\sum_i \rho_i v_i y_i}{\sum_i \rho_i y_i} \qquad (5)$$

Total Energy Balance Equation. The total energy is the sum of the internal, kinetic and potential energies[8]. Then we have,

$$\begin{aligned}\sum_i \frac{\partial(E_i y_i)}{\partial t} = &-\sum_i \frac{\partial}{\partial x}\left[(E_i + p_i) v_i y_i\right] \\ &+ \sum_i \frac{2}{R}\left(E_{i,I} + p_{i,I}\right) v_{i,I} \gamma y_{i,I} \\ &+ \sum_i \rho_i v_i y_i g \sin\theta + \frac{2}{R} q_I (1-\gamma)\end{aligned} \qquad (6)$$

where q represents the conductive heat flux. E_i is the sum of kinetic energy and internal energy, e_i, defined as

$$E_i = \rho_i\left(\frac{1}{2}{v_i}^2 + e_i\right) \qquad (7)$$

Auxiliary Equations. Further relations are needed to solve the governing equations. An inflow rate is determined by the pressure difference between reservoir pressure and wellbore pressure and given as

$$\int_{\Delta x} 2\pi R\gamma v_I \, dx = J\left(p_R - p\right) \qquad (8)$$

where p_R is the pressure at the assumed constant-pressure boundary at some fixed distance from the well and J is the productivity index for the length Δx that can be estimated from reservoir properties. The formation temperature can be estimated simply by assuming a linear temperature change with the depth. Knowing the temperature at some reference datum, formation temperature is given as

$$T_f = T_{ref} + GZ \qquad (9)$$

where G is the geothermal temperature gradient and Z is the vertical distance from the reference. The heat flux from the formation can be written as

$$q_I = U\left(T_f - T\right) \qquad (10)$$

where U is the overall heat transfer coefficient. U depends on the flow rate, type of fluid and completion.

Model Solution. We have introduced the working equations and auxiliary equations to be solved for the flow rate, pressure and temperature profiles. In general for typical production, changes in inflow occur at a much slower rate than the rate at which data is accumulated. Hence, unless there is a large perturbation of the flow (temporally or spatially) we can assume steady-state flow inside the wellbore. The steady-state mass balance equation is

$$\frac{d(\rho_i v_i y_i)}{dx} = \frac{2\gamma y_{i,I}}{R} \rho_{i,I} v_{i,I} \qquad (11)$$

See Appendix A for detailed derivation of the steady-state equations. The momentum balance equation in term of pressure gradient is,

$$\frac{dp}{dx} = -\frac{\rho_m {v_m}^2 f_m}{R} - \frac{d\left(\rho_m {v_m}^2\right)}{dx} - \rho_m g \sin\theta \qquad (12)$$

The energy balance equation will be

$$\begin{aligned}\frac{dT}{dx} = &\frac{2}{R}\left[\gamma \frac{\left(\rho v C_p\right)_{T,I}}{\left(\rho v C_p\right)_T} + (1-\gamma)\frac{U}{\left(\rho v C_p\right)_T}\right]\left(T_f - T\right) \\ &+ \frac{\left(\rho v C_p K_{JT}\right)_T}{\left(\rho v C_p\right)_T}\frac{dp}{dx} + \frac{(\rho v)_T}{\left(\rho v C_p\right)_T} g \sin\theta\end{aligned} \qquad (13)$$

where

$$(\rho v)_T = \sum_i \rho_i v_i y_i \qquad (14)$$

$$\left(\rho v C_p\right)_T = \sum_i \rho_i v_i y_i C_{p,i} \qquad (15)$$

$$\left(\rho v C_p K_{JT}\right)_T = \sum_i \rho_i v_i y_i C_{p,i} K_{JT,i} \qquad (16)$$

The equations can be solved numerically by discretizing the equations with finite differences. The simultaneous solution must be iterative since the equations are nonlinear and coupled. First we assume pressures and temperatures are known for every segment, then the flow rates are calculated with assumed pressures and temperatures. We update temperature and pressure with calculated flow rate, and iterate until the pressure and temperature converge. The details are shown in Appendix B. Unless we say otherwise, the wellbore is discretized into segments with a length of 20 ft.

As the boundary conditions, no flow and no heat transfer are assumed at the very end of the well (toe). Either the bottom hole or the toe pressure is assumed known.

Results and Discussion

From the prediction model developed, we can obtain temperature and pressure profiles along a horizontal wellbore. We use some examples to illustrated how the model can be used to interpret flow profiles from temperature and pressure profiles. We consider two kinds of wells, both having lengths of 2000 ft. One well is completed open hole and the other well has a perforated or slotted liner completion. Both wells are horizontal. The open hole well produces from the entire wellbore, while the perforated/slotted well can be shut off certain sections. For the open hole completion, wall friction is relatively large because of large wall roughness. It also has a higher heat transfer coefficient between the formation and the wellbore because the wellbore is bare. On the other hand, the pipe roughness for a perforated/slotted completion is less and the heat transfer coefficient largely depends on what materials surround the wellbore such as steel casing or cement. The details about the wells are listed in Tables 1 and 2. We assume that the well fully penetrates the reservoir at the center and the reservoir formation is homogeneous (i.e. productivity index is uniform along well). The reservoir and fluid properties are listed in Tables 3 and 4.

Completion Effects for Oil Production

As a first comparative example, we assume that both completions produce single phase oil from the entire section. Reservoir properties are the same for both cases. Because of the larger wall friction, pressure loss in the open hole well is higher and the total production is larger. To have the same amount of total production for a perforated/slotted well as for the open hole case (this allows better comparisons between the cases), the pressure at the toe of the perforated/slotted well was set lower than that of the open hole well.

Fig. 2 shows the inflow rate profiles for both cases. As can be seen, the inflow rate shows a quadratic increase from the toe to the heel. Figs. 3 and 4 show the flow rate and pressure profiles respectively. For the open hole well, a rapid pressure decrease occurs. The temperature profiles, presented in Fig. 5, also show a quadratic increase. However, the changes are not simply proportional to the flow rate since this increase is partly caused by pipe friction. The fluids expand because of frictional pressure loss, and gain temperature because of Joule-Thomson effects. From these effects the obtained heat will be proportional to the flow rate; however, the fluids lose heat to the formation because of the conductive heat transfer. For the open hole wellbore, the heat transfer rate is higher than the perforated/slotted liner well. Consequently, the open hole wellbore gains more heat and loses more temperature to the formation. The net temperature increases for both are almost the same, about 0.8 ^{o}F, although the shapes of the curves are different.

Production Interval Effects for Oil Production

We will show examples with non-uniform production intervals to see how they affect the profiles. Again we consider the well described in Table 2, but now compare with a well assumed to have two distinct shut off zones as illustrated in Fig. 6. The inflow rate per 20 ft for both cases are shown in Fig. 7 and the flow rates profiles are displayed in Fig. 8. We doubled the productivity index for the non-uniform production intervals case to obtain of the same total production as the previous case.

The pressure profile of the well with intervals (Fig. 9) indicates slope changes at the production sections. The temperature profile (Fig. 10) behaves more interestingly. The overall temperature increase of the production interval case is about 1.6 ^{o}F which is higher than without intervals. This is because of the larger pressure drop. However, the more important finding here is the anomalous behavior of the temperature curve. The temperature curve shows more sensitivity to the location of the production zones than does the pressure profile. The interval production causes sudden slope changes on the temperature curve that indicate where the inflow occurs or not. This observation suggests that the temperature profile can be useful in identifying the discontinuous production.

Joule-Thomson Cooling and Production Intervals Effects for Gas Production

In this example, we consider gas production with and without shut off zones. We will see how Joule-Thomson cooling affects the temperature profile through the pressure drop. The reservoir and fluid properties are listed in Table 4. For the well with shut off zones, the permeability was set 30 md higher than the well without shut off zones to have similar amount of total production. Fig. 11 shows the flow rate profiles. The pressure profiles are shown in Fig. 12.

The pressure profile with intervals has a similar curve to that from the oil production case. However, the temperature behavior (Fig. 13) shows much higher sensitivity to the pressure loss than for oil, decreasing about 3 ^{o}F throughout the 2000 ft wellbore length. As the pressure decreases, the gas expands and the temperature decreases because of Joule-Thomson cooling. Analogous to the oil production case, when the gas entered in discrete intervals, the pressure profile shows relatively small discontinuities and the temperature profile shows more significant anomalies. The temperature curve is more sensitive to the production discontinuity as pointed out in the previous example and this change is more noticeable in gas production than in oil production.

Elevation Effects

Elevation changes affect both pressure and temperature. Pressure drops more in upward flow and less in downward flow because of gravity. Temperature is also affected by gradual change of geothermal temperature.

For this example, the geothermal gradient is taken to be 0.01 ^{o}F/ft. Inclinations of +2^{o} and -2^{o} from horizontal were examined. This is a very small inclination, and it is very common in the field to have such an inclined angle in a nominally horizontal well. We will see how these small inclinations affect both profiles. The first run is the same condition as the previous perforated/slotted well case (Table 2 and 3) except for the inclinations. The pressure and temperature profiles of upward flow and downward flow are shown in Figs. 14 and 15 compared with the base case (perforated/slotted well without inclination case).

As expected, the pressure drop of upward flow is more than the base case and the pressure drop of downward flow is less. In downward flow, the wellbore encounters warmer formation temperature and the overall temperature increase is higher than the base case. Upward flow temperature behavior is more profound. The fluid temperature decreases because of a cooler environment, and increases because of Joule-Thomson heating. This results in the temperature profile having a minimum between the toe and the heel. This shape is very remarkable since temperature should never decrease in a perfectly horizontal wellbore producing liquid. This downward concave shape could be an identification of the upward trajectory of the well and illustrates that an accurate measurement of well trajectory is needed to interpret temperature and pressure profiles in nominally horizontal wells.

For gas production, the results were generated under the same condition as the perforated/slotted gas production case (Table 2 and 4) except for the inclinations. Comparisons with the base case are displayed in Figs. 16 and 17.

Theoretically, the pressure drop is smaller in downward flow and larger in upward flow. However, because of the relatively small gas density, these effects hardly appear in the pressure profiles. Meanwhile the temperature profiles show distinct differences for the two inclinations. Because of Joule-Thomson cooling, the usual temperature profile shows a monotonically decreasing curve in gas production. But in downward flow, the temperature increases and reaches the highest value around 1500 ft from the heel, and then decreases.

Water Entry Effects

Often, it has been said that entering water has warmer temperature than entering oil because water is produced from deeper zone due to the water coning or the existence of the water compartment. Since we consider that the inflow temperature is only a function of the wellbore depth in this study, the water enters with the same temperature as the oil unless there is inclination of the well. Therefore what we will discuss here is only the effect of the wellbore flow.

We show comparisons of two-phase oil and water production case with the single phase oil production case. The first scenario has a water entry from the heel for 400 ft as shown in Fig. 18. The pressure and temperature profiles are shown in Figs. 19 and 20 with the single phase case. The pressure profiles with or without water production are almost identical which tells us that the water entry cannot be identified from the pressure profile at least for this case. Meanwhile, the temperature profile shows the difference between the cases of with water and without water. Knowing what the temperature profiles look like in the single phase case, the location of water entry can be detected. Next, we consider the water production from the toe for 400 ft as shown in Fig. 21. Since we again observed the same pressure profiles, only the temperature profiles are shown in Fig. 22. From the figure we can see the slope change where the water entry starts. However, we cannot easily see the location where the water entry ends. As a last example, the case of water entry between at 800 ft to 1200 ft from the heel is considered. The flow rate profiles are displayed in Fig. 23 and the temperature profiles are shown in Fig. 24. The start of the water production interval is identified as the location where the two curves diverge. This suggests that water production might be identifiable by comparing a measured temperature profile with a calculated single-phase profile. Although it is small, there is a slope change at the end of the water production (800 ft from the heel).

The wellbore temperature is the accumulated information that contains all information up to the point it is measured. From above examples, we can say that the temperature profiles contain more information about water entry when the water entry occurs closer to the heel. And as the water entry occurs further away from the heel, the temperature profiles lose information about the location of water entry.

Conclusions

We have presented a temperature and pressure prediction model that can be used for the interpretation of temperature changes along horizontal wells. Unlike vertical wells, temperature and pressure changes in horizontal wells are very delicate and are affected by small changes in surrounding conditions. Conclusions from various examples are as follows:

1. For single-phase oil production, the overall temperature changes are small even at large flow rates and for small pipe diameter. Measured changes would probably be difficult to interpret. However, even though the temperature change is small, it is possible that combining it with other information would make inflow interpretation possible.
2. Single-phase gas production has very clear features in the temperature profile. This is because the pressure in the gas phase changes less than that of oil, and gas, being compressible, is more affected by Joule-Thomson cooling. Thus, the temperature profiles in a gas have more interpretable information than oil wells. There is less need for pressure information as well.
3. Intervals of produced oil or gas leave clear marks on the temperature profiles, and these marks on the temperature profiles can be used to identify the fluid entry location.
4. Certain well trajectories (downward and upward) create features in temperature profiles, such as temperature minima between the toe and the heel of a well, that provide useful information for interpreting the flow profile from temperature profile.
5. The pressure profiles for single phase oil production and oil-water two-phase production are almost the

same. There are differences only in the temperature profiles. Compared with a single-phase temperature curve, the water entry zone may be detectable.

Nomenclature

C_p = heat capacity
e = internal energy per unit mass
f = friction factor
g = gravity acceleration
G = geothermal gradient
H = enthalpy per unit mass
i = phase
J = productivity index
j = segment number
K_{JT} = Joule-Thomson coefficient
p = pressure
p_R = average reservoir pressure
q = heat flux
R = pipe radius
T = temperature
T_f = formation temperature
T_{ref} = reference temperature
U = overall heat transfer
v = velocity
y = hold up
Z = depth
γ = pipe opening ratio
ρ = density
θ = angle
τ = stress shear

Subscript

i = phase
I = inflow property
m = mixture property
T = total property

Acknowledgements

This work is supported by the U.S. Department of Energy NETL Contract DE-FC26-03NT15402. A. D. Hill holds the R. W. Whiting Endowed Chair at Texas A&M University. Larry W. Lake holds the W.A. (Monty) Moncrief Chair at The University of Texas.

References

1. Ramey, H.J., Jr.: "Wellbore Heat Transmission," Journal of Petroleum Technology, Trans. AIME volume 225, pp. 427-435, April 1962.
2. Sagar, R.K., Dotty, D.R., and Schmidt, Z.: "Predicting Temperature Profiles in a Flowing Well," paper SPE 19702, November 1991.
3. Hasan, A.R. and Kabir, C.S.: *Fluid Flow and Heat Transfer in Wellbores*, Society of Petroleum Engineers, Richardson, TX, 2002.
4. Dikken, B.J.: "Pressure Drop in Horizontal Wells and Its Effect on Production Performance", JPT, November 1990.
5. Yuan, H., Sarica, C., and Brill, J.P.: "Effect of Completion Geometry and Phasing on Single-Phase Liquid Flow Behavior in Horizontal Wells" paper SPE 48937, September 1998
6. Ouyang, L.-B., Arbabi, A. and Aziz, K.: "A Single-Phase Wellbore-Flow Model for Horizontal, Vertical, and Slanted Wells." Paper SPE 36608, October 1998.
7. Hill, A.D.; *Production Logging-Theoretical and Interpretive Elements*, Society of Petroleum Engineers Inc., Richardson, TX, 1990
8. Bird, R. B., Stewart, W.E., and Lightfoot, E.N.; *Transport Phenomena*, second edition, John Wiley and Sons, New York, NY, 2002.

Appendix A: Derivation of the Governing Equations in Steady State Flow

The objective of this Appendix is to derive the working equations that is being solved in this paper. The steady-state mass balance, Eq. 2, is given as

$$0 = -\pi R^2 \frac{d(\rho_i v_i y_i)}{dx} + 2\pi R \gamma \rho_{i,I} v_{i,I} y_{i,I} \tag{A-1}$$

Dividing by πR^2 yields

$$\frac{d(\rho_i v_i y_i)}{dx} = \frac{2\gamma y_{i,I}}{R} \rho_{i,I} v_{i,I} \tag{A-2}$$

The steady-state momentum balance, Eq.3, is

$$0 = -\frac{2\tau_w}{R} - \frac{d\left(\rho_m {v_m}^2 + p\right)}{dx} - \rho_m g \sin\theta \tag{A-3}$$

The shear stress at the wall τ_w is

$$\tau_w = \frac{\rho_m f_m v_m^2}{2} \tag{A-4}$$

Where f_m is a friction factor. Substituting into Eq. A-3 and solving for pressure gradient give

$$\frac{dp}{dx} = -\frac{\rho_m {v_m}^2 f_m}{R} - \frac{d\left(\rho_m {v_m}^2\right)}{dx} - \rho_m g \sin\theta \tag{A-5}$$

The energy balance Eq. 6 with the substitution of Eq. 7 is

$$\begin{aligned} 0 = &-\sum_i \frac{d}{dx}\left[\left(\rho_i e_i + \rho_i \frac{1}{2} {v_i}^2 + p_i\right) v_i y_i\right] \\ &+ \sum_i \frac{2}{R}\left(\rho_i e_{i,I} + \rho_i \frac{1}{2} {v_{i,I}}^2 + p_{i,I}\right) vi,_I \gamma y_{i,I} \\ &+ \sum_i \rho_i v_i y_i g \sin\theta + \frac{2}{R} q_I (1-\gamma) \end{aligned} \tag{A-6}$$

The relationship between internal energy and enthalpy is

$$H = e - \frac{p}{\rho} \tag{A-7}$$

From the results of numerical simulation, the kinetic energy terms are negligible. Substituting Eq. A-7 into A-6 and neglecting kinetic energy terms yields

$$\begin{aligned} 0 = &-\sum_i \frac{d}{dx}(\rho v_i H_i y_i) + \sum_i \frac{2}{R} \rho v_i H_{i,I} y_i v_{i,I} \gamma y_{i,I} \\ &+ \sum_i \rho_i v_i y_i g \sin\theta + \frac{2}{R} q_I (1-\gamma) \end{aligned} \tag{A-8}$$

From the mass balance Eq. A-2, we have

$$\frac{d(\rho_i v_i y_i H_i)}{dx} = \rho_i v_i y_i \frac{dH_i}{dx} + H_i \frac{d(\rho_i v_i y_i)}{dx} = \rho_i v_i y_i \frac{dH_i}{dx} + H_i \frac{2}{R} \gamma y_{i,I} \rho_{i,I} v_{i,I} \quad \text{(A-9)}$$

Substituting Eq. A-9 into A-8 gives

$$\sum_i \rho_i v_i y_i \frac{dH_i}{dx} = \frac{2}{R} \sum_i \rho_{i,I} v_{i,I} \gamma y_{i,I} (H_{i,I} - H_i) + \frac{2}{R} q_I (1-\gamma) + \sum_i \rho_i y_i v_i g \sin\theta \quad \text{(A-10)}$$

Since the enthalpy is a function of temperature and pressure, its derivative can be expanded as

$$\frac{dH_i}{dx} = C_{p,i} \frac{dT_i}{dx} + \frac{1}{\rho_i}(1 - \beta_i T_i) \frac{dp_i}{dx} = C_{p,i} \frac{dT_i}{dx} - C_{p,i} K_{JT,i} \frac{dp_i}{dx} \quad \text{(A-11)}$$

$H_{i,I}$ is the enthalpy of inflowing fluid and we have assumed that the pressure difference between the inflowing fluid and the wellbore is negligible. Then, the difference of enthalpy will be

$$H_{i,I} - H_i = C_{p,i} (T_{i,f} - T_i) \quad \text{(A-12)}$$

Substituting Eq. A-11 and A-12 into Eq. A-10 gives

$$\sum_i \rho_i v_i y_i C_{p,i} \frac{dT_i}{dx} - \sum_i \rho_i v_i y_i C_{p,i} K_{JT,i} \frac{dp_i}{dx} = \frac{2}{R} \sum_i \rho_{i,I} v_{i,I} \gamma y_{i,I} C_{p,i} (T_{i,f} - T_i) + \frac{2}{R} q_I (1-\gamma) + \sum_i \rho_i y_i v_i g \sin\theta \quad \text{(A-13)}$$

If each phase has the same pressure and temperature, Eq. A-13 becomes

$$\frac{dT}{dx} \sum_i \rho_i v_i y_i C_{p,i} = \frac{dp}{dx} \sum_i \rho_i v_i y_i C_{p,i} K_{JT,i} + \frac{2}{R}(1-\gamma) q_I + \frac{2}{R} \sum_i \rho_{i,I} v_{i,I} \gamma y_{i,I} C_{p,i} (T_f - T) + \sum_i \rho_i v_i y_i g \sin\theta \quad \text{(A-14)}$$

Substituting Eq. 10 and solving for temperature gradient yield

$$\frac{dT}{dx} = \frac{2}{R} \left[\gamma \frac{(\rho v C_p)_{T,I}}{(\rho v C_p)_T} + (1-\gamma) \frac{U}{(\rho v C_p)_T} \right] (T_f - T) + \frac{(\rho v C_p K_{JT})_T}{(\rho v C_p)_T} \frac{dp}{dx} + \frac{(\rho v)_T}{(\rho v C_p)_T} g \sin\theta \quad \text{(A-15)}$$

Appendix B: Solution Procedure

This Appendix gives the procedure of numerical solution of the working equations for the single-phase of oil or gas flow. Solving the multiphase flow case requires another relationship for holdups.

The mass balance equation can be discretized by backward finite difference method as

$$v_j + A_j v_{j-1} = B_j \quad \text{(B-1)}$$

where

$$A_j = -\frac{\rho_{j-1}}{\rho_j} \quad \text{(B-2)}$$

$$B_i = \frac{(\rho_I)_{j-1}}{\rho_j} \frac{J_j (p_R - p_j)}{\pi R^2} \quad \text{(B-3)}$$

and j is a segment number that indicates position along the well. The discretized momentum balance equation will be similarly,

$$p_j - p_{j-1} = C_j \quad \text{(B-4)}$$

where

$$C_j = \Delta x \left[-\frac{\rho_j {v_j}^2 f_j}{R} - \rho_j g \sin\theta_j \right] - \left[(\rho v)_j{}^2 - (\rho v)_{j-1}{}^2 \right] \quad \text{(B-5)}$$

The energy balance equation can be discretized as

$$D_j T_j - T_{j-1} = E_j \quad \text{(B-6)}$$

where

$$D_j = 1 + \frac{2\Delta x}{R \rho_j v_j} \left\{ (\rho_I)_j (v_I)_j + \frac{U_j}{(C_P)_j} \right\} \quad \text{(B-7)}$$

$$E_j = \Delta x \left[(K_{JT})_j \left(\frac{dp}{dx} \right)_j - \frac{1}{(C_P)_j} g \sin\theta_j + \frac{2}{R \rho_j v_j} \left\{ (\rho_I)_j (v_I)_j + \frac{U_j}{(C_P)_j} \right\} (T_f)_j \right] \quad \text{(B-8)}$$

To solve these equations simultaneously we first guess all the values of pressures and temperature for every segment, and obtain the velocity profile from Eq. B-1. Then, we calculate the temperature profile from Eq. B-8 and repeat this procedure until the assumed values and calculated values match. After obtaining the convergence on temperature, we repeat the same iteration on the pressure profile. The flow chart of this procedure is shown in Fig. 25. Convergence is rapid because temperature and pressure changes are ultimately small.

Table 1. Open hole wellbore description

Pipe Inner Diameter [in]	2.259
Wellbore Length [ft]	2000
Inclination [°]	0
Relative Roughness	0.027

Table 2. Perforated/Slotted wellbore description

Pipe Inner Diameter [in]	2.259
Pipe Outer Diameter [in]	2.529
Wellbore Length [ft]	2000
Inclination [°]	0
Relative Roughness	1.E-03
Thermal Conductivity of Pipe [Btu/hr ft °F]	6.934

Table 3. Reservoir and Fluid Properties of Oil

Formation Temperature at the toe [°F]	180
Average Reservoir Pressure [psi]	6000
Permeability [md]	120
Thermal conductivity of fluid and formation [Btu/hr ft °F]	2
Width of Reservoir [ft]	3000
Length of Reservoir [ft]	2000
Thickness of Reservoir [ft]	50
Heat Capacity [Btu/lb°F]	0.528
Density [lb/ft^3]	50
Solution Gas-Oil Ratio [SCF/STB]	800
Thermal Conductivity of fluid [Btu/hr ft °F]	0.797

Table 4. Reservoir and Fluid Properties of Gas

Formation Temperature at the toe [°F]	180
Average Reservoir Pressure [psi]	1200
Permeability [md]	10
Thermal conductivity of fluid and formation [Btu/hr ft °F]	1.3
Width of Reservoir [ft]	3000
Length of Reservoir [ft]	2000
Thickness of Reservoir [ft]	50
Heat Capacity [Btu/lb °F]	0.39999
Specific Gravity	0.75
Thermal Conductivity of fluid [Btu/hr ft °F]	0.01156

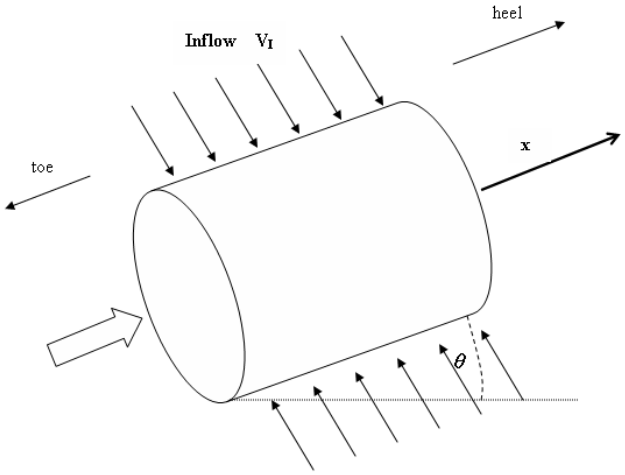

Fig. 1 Differential volume element of a wellbore

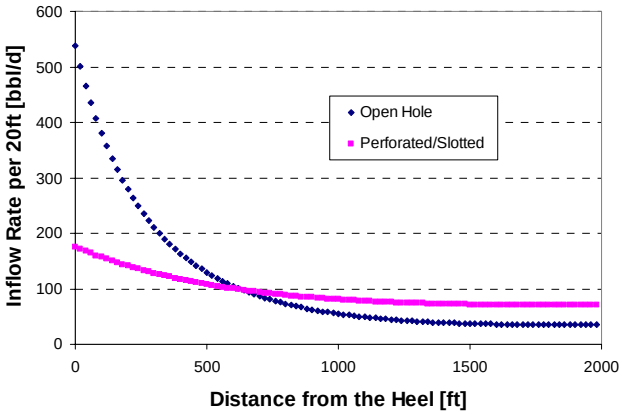

Fig. 2 Inflow rate profiles (open hole and perforated/slotted well)

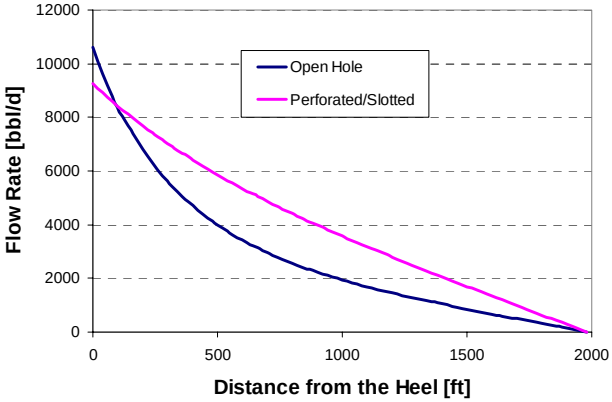

Fig.3 Accumulated flow rate profiles (open hole and perforated/slotted well)

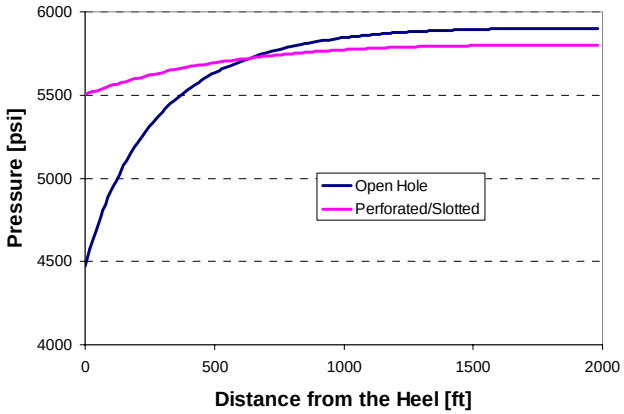

Fig. 4 Pressure profiles (open hole and perforated/slotted well)

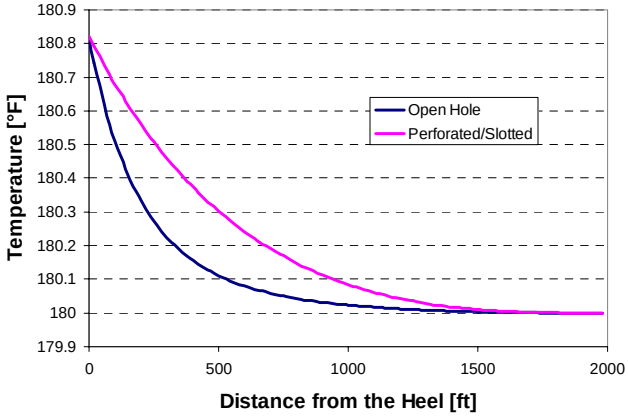

Fig. 5 Temperature profiles (open hole and perforated/slotted well)

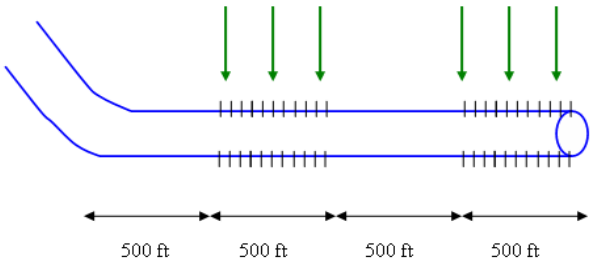

Fig. 6 Inflow profile

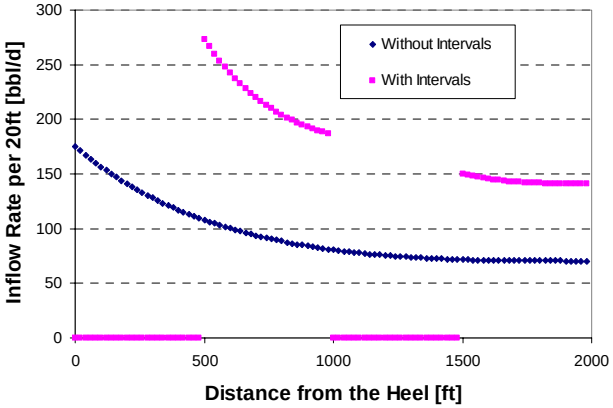

Fig. 7 Inflow rate profiles (with/without oil production intervals)

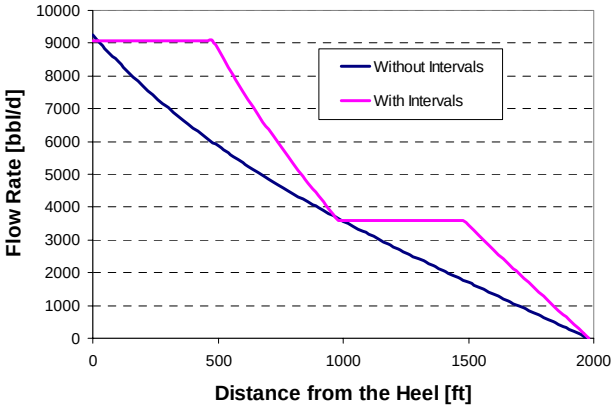

Fig. 8 Accumulated flow rate profiles (with/without oil production intervals)

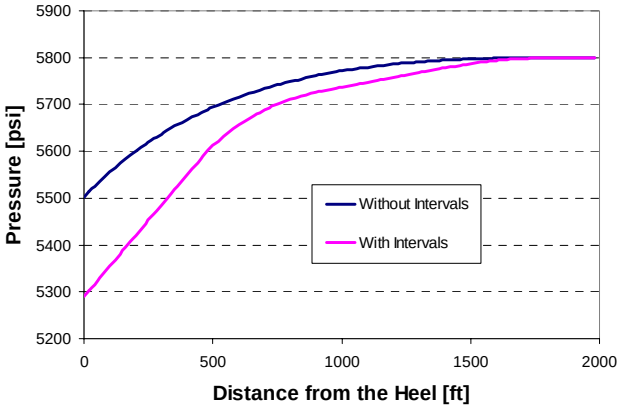

Fig. 9 Pressure profiles (with/without oil production intervals)

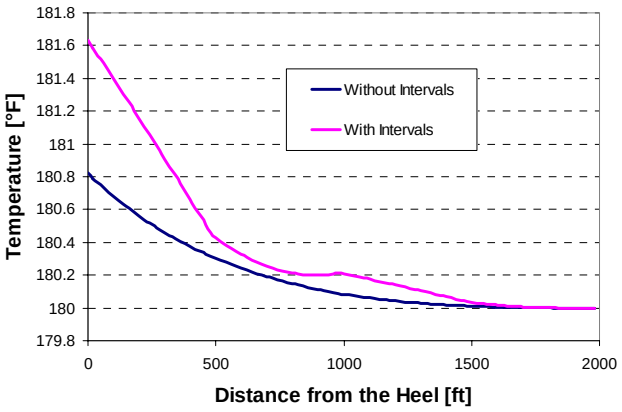

Fig. 10 Temperature profiles (with/without oil production intervals)

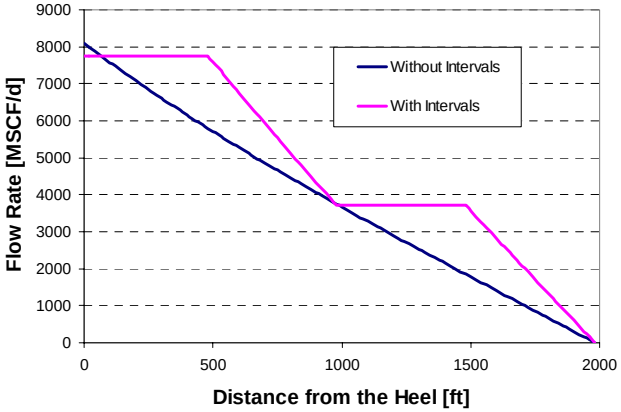

Fig. 11 Accumulated flow rate profiles (with/without gas production intervals)

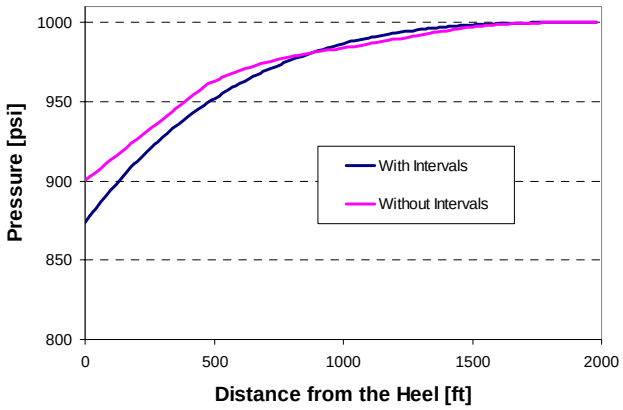

Fig. 12 Pressure profiles (with/without gas production intervals)

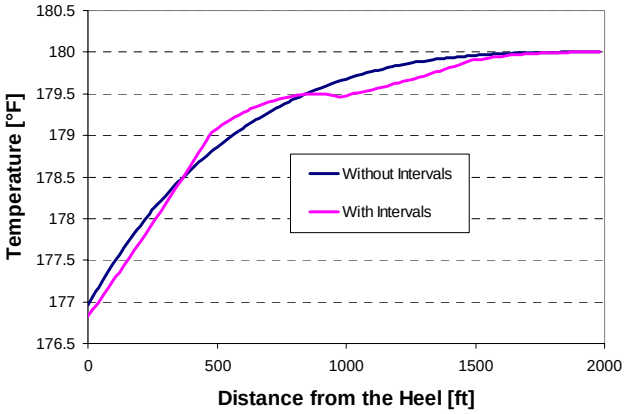

Fig. 13 Temperature profiles (with/without gas production intervals)

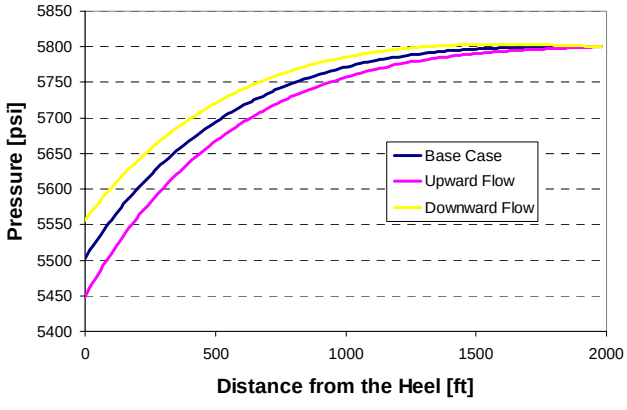

Fig. 14 Pressure profiles with inclinations (perforated/slotted well oil production)

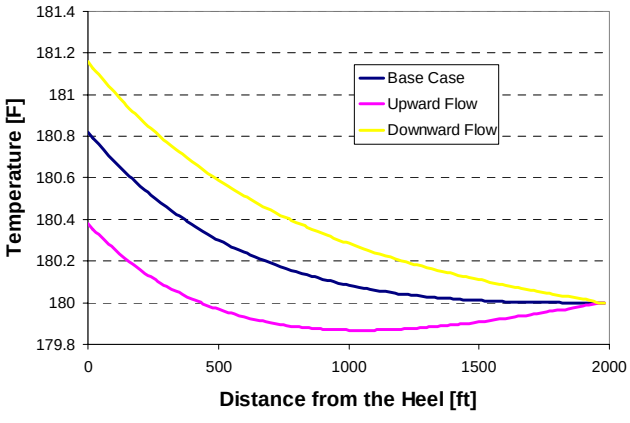

Fig. 15 Temperature profile with inclinations (perforated/slotted well oil production)

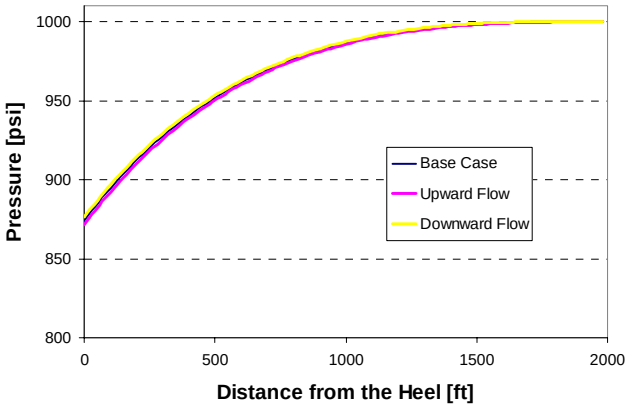

Fig. 16 Pressure profiles with inclinations (perforated/slotted well gas production)

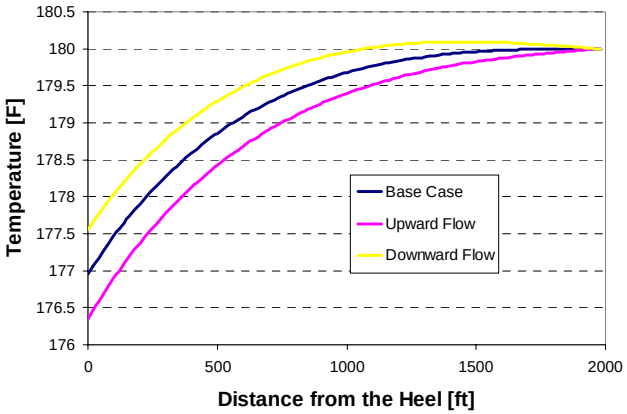

Fig. 17 Temperature profiles with inclinations (perforated/slotted well gas production)

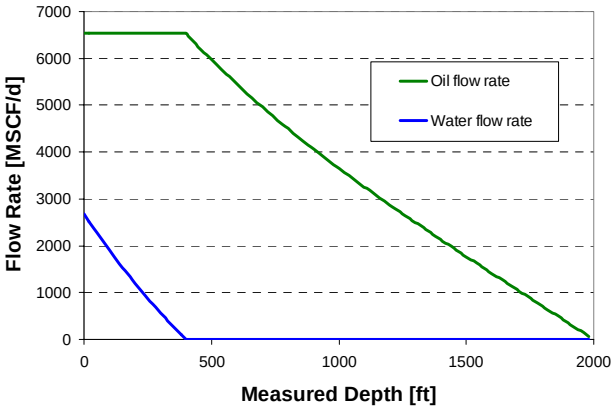

Fig. 18 Accumulated flow rate profiles (oil and water production)

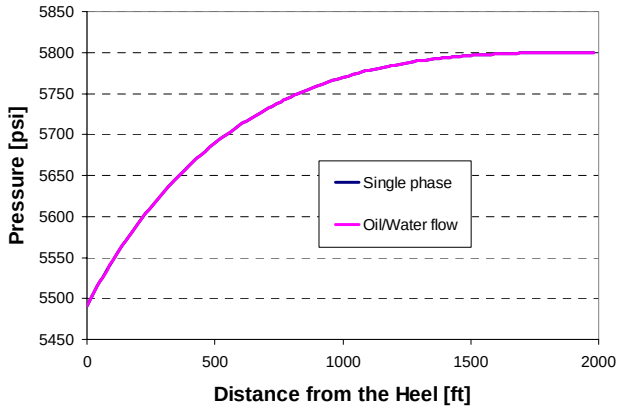

Fig. 19 Pressure profiles comparison (oil and water production)

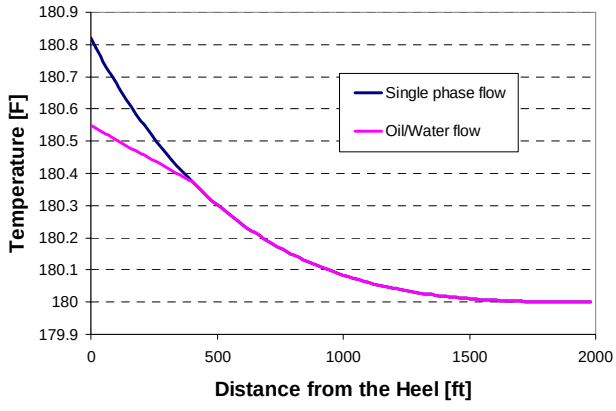

Fig. 20 Temperature profiles comparison (oil and water production)

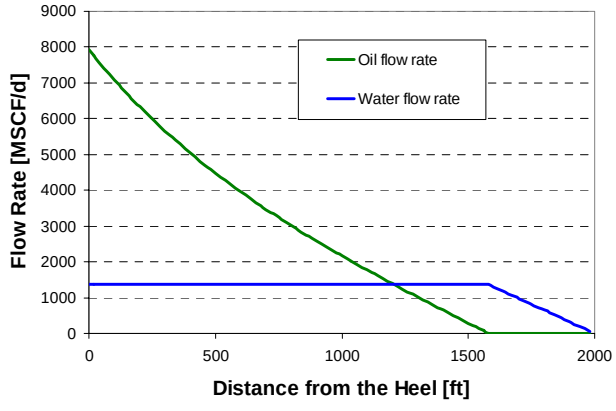

Fig. 21 Accumulated flow rate profiles for oil and water (oil and water production)

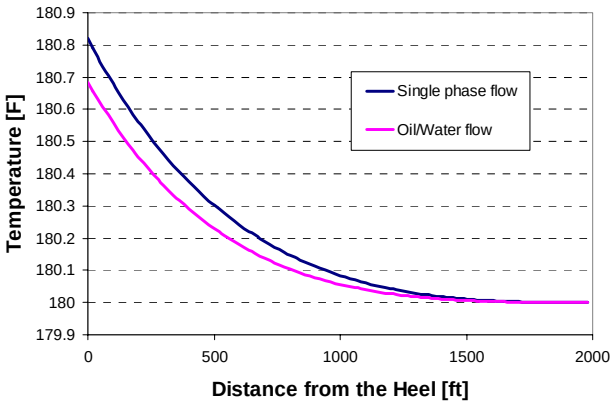

Fig. 22 Temperature profiles comparison (oil and water production)

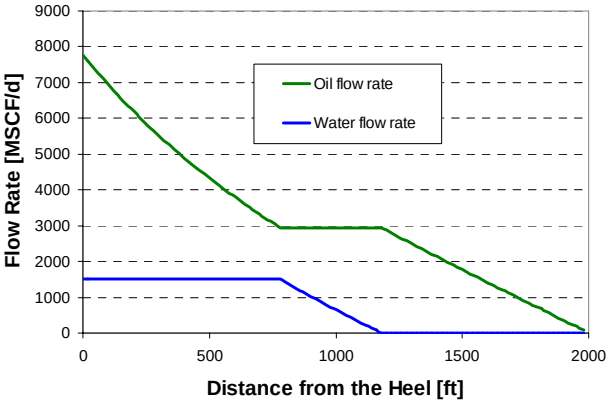

Fig. 23 Accumulated flow rate profiles for oil and water (oil and water production)

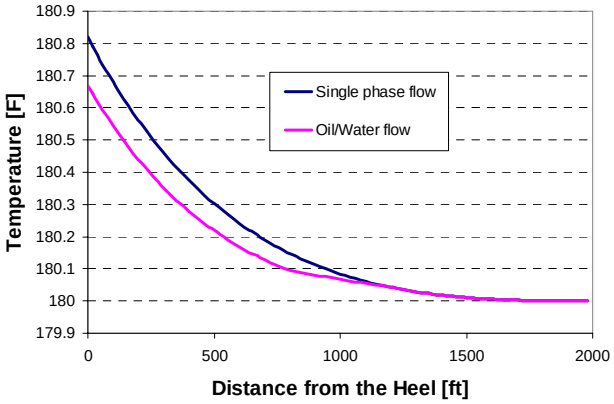

Fig. 24 Temperature profiles comparison (oil and water production)

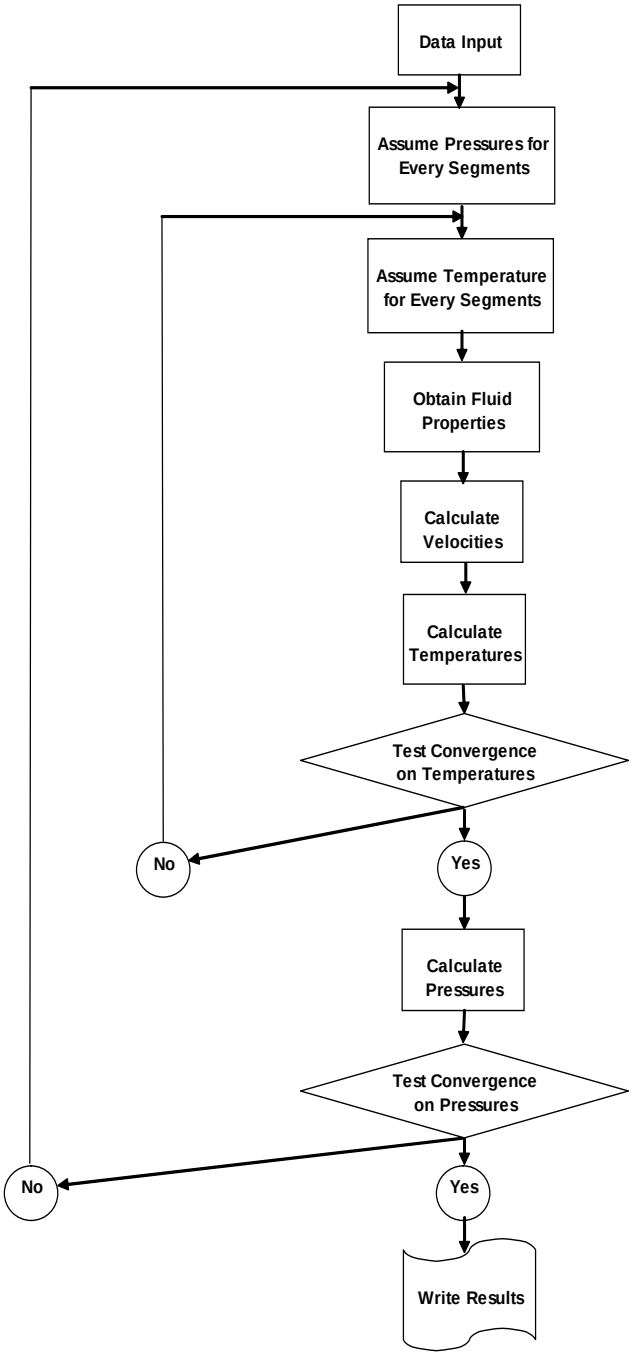

Fig. 25 Flow chart of the solution procedure